

*Master in Photonics*

**MASTER THESIS WORK**

**STUDY OF FEMTOSECOND LASER BEAM  
FOCUSING IN DIRECT-WRITE SYSTEM**

**Albert Van Eeckhout Alsinet**

**Supervised by Dr. Juan Marcos Fernandez Pradas (UB), Dr. Salvador Bosch  
(UB)**

Presented on date 22<sup>th</sup> July 2016

Registered at

**ETSETB** Escola Tècnica Superior  
d'Enginyeria de Telecomunicació de Barcelona

# Study of femtosecond laser beam focusing in direct-write system

**Albert Van Eeckhout Alsinet**

Grup de processament de materials amb làser, Departament de Física Aplicada, Universitat de Barcelona, Martí i Franquès 1, Barcelona 08028, Spain

E-mail: 41bert@gmail.com

**Abstract.** Direct-write techniques appear as a versatile option in rapid-prototyping applications because they can directly transfer a custom pattern from a digital file. Lasers are a distinguished tool which allow to perform non-contact direct-write techniques with the ability to add, remove and modify different types of materials. Moreover, they have a high focusing power and offer high spatial resolution when a femtosecond laser is used due to the reduction of thermal effects. Additive and subtractive techniques can be performed in one laser-based direct-write system with minimum variations in the setup. In all cases, properties of the laser beam, such as the beam width or the morphology of the intensity distribution have an effect on the results of the laser processing. The aim of this work is the study of the laser propagation in a specific laser-based direct-write setup. The beam intensity distribution effects are measured at different positions and compared with simulations. The influence of the main parameters, pupil displacement and objective tilt, on the morphological properties of the intensity distribution is analysed. Well defined spots with good reproducibility are obtained. In addition, at comparing the simulation with the experiments, the origin of some morphological properties are reported and they can be used to optimize the setup.

**Keywords:** Gaussian beam propagation, femtosecond laser, laser direct-write, beam simulation

## Introduction

Direct-write techniques are widely used in rapid-prototyping applications because they are faster and less expensive than alternative technologies. They offer the possibility to transfer a custom pattern from a digital file. Lasers are an outstanding tool, which are able to remove, modify or add material [1]. Moreover, lasers avoid any mechanical contact and have interesting properties such as high focusing power which allows to obtain high degrees of integration. Furthermore, the use of femtosecond lasers drastically reduces thermal effects thanks to its ultrashort pulse duration guaranteeing the best resolution. Therefore, it provides higher resolution than other extended technologies when a femtosecond laser is used. Femtosecond lasers are also able to promote non-linear processes. These non-linear processes, as second harmonic generation (SHG), are produced only in the high intensity zone near the focus. Therefore, the process brings higher resolution than other extended technologies.

Each different application is interested in different properties of the laser, such as resolution capability, intensity or morphology of the intensity distribution. For example, when the laser beam

profile is Gaussian, the intensity of the beam decreases with the radial distance following the Gaussian distribution. Thus, at ablating materials, the ablated area increases with the pulse energy. The use of Gaussian beams allows to ablate the material below the diffraction limit and obtain spots much smaller than this limit [2]. Then, Gaussian beams are convenient when high miniaturization is sought. Another interesting kind of beams are flat-top beams which ideally have a square intensity distribution where the top of the beam is flat. These beams produce a flat ablation in depth. They are used when a 3D material is ablated and we want to ablate down to a certain depth. Thus, flat-top lasers are used in direct-write lithography processes where this intensity distribution is the optimal.

This work is focused in studying the laser propagation in the direct-write setup shown in figure 1(a). It allows to modify and measure each laser pulse energy individually, therefore, being very useful at developing experiments. This setup is very versatile because it can be used to implement many different direct-write techniques. This setup has been used to make LIFT [3], to ablate 3D polymers [2] or thin films as in this study by only changing the substrate. In order to determine the different laser properties and its propagation, several research have been done using this laser [2,3]. These works determine the beam intensity profile from the ablation of materials. However, the evolution of the beam is not the only interesting feature, it is also interesting to determine the factors that produce this evolution. The usual way to determine these factors is comparing the theory with the reality using simulations [4].

The difference between this work and the previous ones is the focus in the intensity distribution. In this study, the intensity distribution is studied in more detail to obtain the most accurate simulation that matches the reality. It is not only focused in the beam width at different positions, it is also focused in the intensity distribution. The aim of this work is the study of the laser propagation in the laser-based direct-write setup. The effects of the beam intensity distribution are measured in different positions and compared with the simulations. When the intensity distribution of a beam at all positions is known, it would be possible to optimize the setup finding the most efficient position. Moreover, it would be also possible to detect defects on the setup and solve them by optimizing again the setup. Defects are usually detected when the simulation is improved to match the reality, and possible misalignments are taken into account. In this work we determine the origin of some changes in the intensity distribution (with respect to the Gaussian beam distribution) from the simulation-reality comparison.

## 1. Experimental

The setup consists of a femtosecond laser, an optical system and a set of xyz translation stages (figure 1(a)). The ablation was carried out through the use of a pulsed ytterbium (Yb:KYW) diode pumped laser (Amplitude Systems, S-pulse), with 1027 nm wavelength and 450 fs pulse duration. The laser beam has a roughly Gaussian intensity distribution (figure 2(a)). The optical system is composed of a crossed polarized attenuator and a beam splitter for energy control and subsequent measurement, followed by a series of mirrors, whose purpose is to guide the laser radiation toward a microscope objective (50x, 0.55NA, 13 mm working distance). The objective tightly focuses the laser beam onto the substrate, a transparent glass slide coated with a titanium thin film with a thickness of around 50 nm, as shown in figure 1(a). A 150  $\mu\text{m}$  coverslip with 0.94 transmissivity is placed above the substrate in order to protect the objective from the titanium ejected particles. The coverslip rests 1 mm above the substrate over two glass spacers. The used glass is transparent at this wavelength and at this position the laser is not focused enough to produce a light-matter interaction. Therefore, the propagation is preserved with the minimum variations because of the no interaction between the glass and the laser beam.

The substrate system was laid on a  $xyz$  translation stage that permitted the precise translation of it with respect to the laser beam. The ablation was carried out in such a way that each single laser pulse was responsible for the ablation of a single spot. After the spot generation, the stage was displaced at a distance of  $50\ \mu\text{m}$  or  $60\ \mu\text{m}$  (depending on the energy used) and another spot was generated on the substrate position until each single row in the microarray was completed.

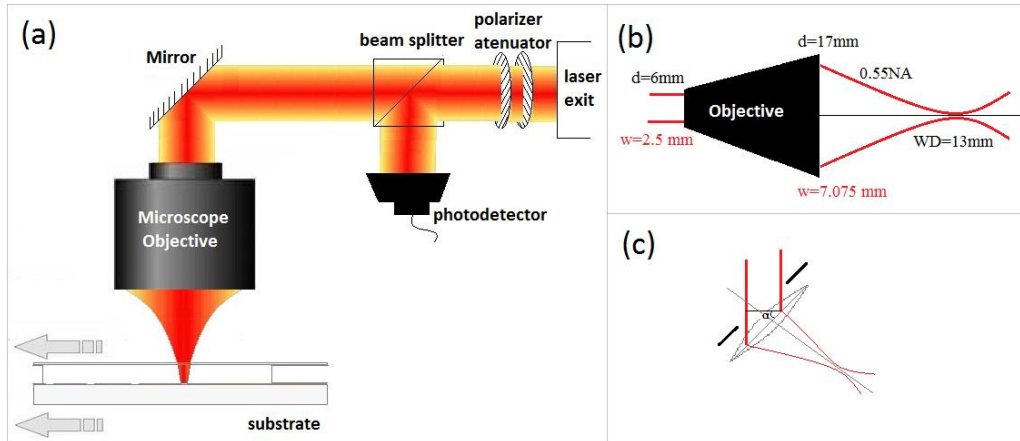


Figure 1. Scheme of (a) the experimental set-up, (b) the laser beam behaviour before and after the objective, (c) the simulation.

In order to align the objective, two micrometric screws on the  $xy$  axis are used, which allow moving the objective in these directions. The produced changes in the intensity profile are observed after the objective. In order to observe the laser beam after the objective, an intensity profile ccd camera is placed below the beam waist, at distances higher than  $1\text{mm}$  with the purpose to do not saturate and damage the camera. It was dimensionally impossible to put the camera at the equivalent position above the waist. We consider the objective aligned when the Gaussian beam is just in the middle of the objective aperture (figure 2(b)). This is achieved by changing the position of the objective using the micrometric screws.

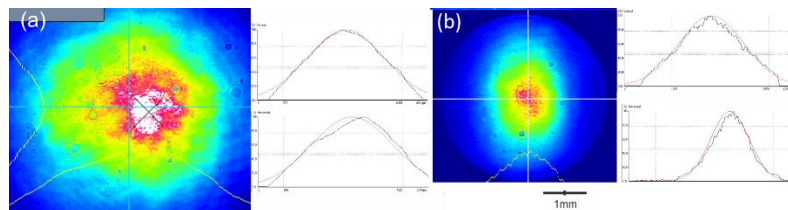


Figure 2. Plot of the Yb:KYW laser beam intensity distribution (a) before the objective (b) around  $3\text{mm}$  below the beam waist. Plot (b) is rotated with respect to the (a) axis.

On the other hand, a program using MATLAB (Appendix A) is developed to simulate the laser beam propagation after the objective. In order to develop the simulation, two approximations were needed because of the types and distances of lenses which are involved in the composition of the complex lens are unknown. In other words, the lens is like a “black box” with  $0.55\text{NA}$ ,  $50\times$ ,  $13\text{mm}$  working distance and  $6\text{mm}$  aperture diameter (figure 1(b)). The first approximation consists on treating the beam as a circular perfectly collimated Gaussian beam (in this case the beam has a flat wavefront) with  $2.5\text{mm}$  of beam width. The second one, the complex lens is reduced to a simple lens which focalize the beam  $13\text{mm}$  below the objective, with a  $0.55\text{NA}$  and with a pupil. Furthermore, the Gaussian beam observed at the output of the objective is  $2.83$  times larger than at the input. In order to simulate it, the beam width is changed from  $2.5\text{mm}$  to  $7.075\text{mm}$ . Moreover, the beam propagates through an aperture and this aperture is simulated to be  $17\text{mm}$  in diameter ( $2.83$  times  $6\text{mm}$  which is the real value at the objective’s entrance). The

simulation also contemplates the possibility of having a tilt angle between the objective direction and the beam propagation direction.

The program starts defining the known parameters: wavelength, aperture radius, beam width, energy pulse, titanium fluence threshold, pulse duration, speed of light multiplied by the electrical permittivity of vacuum, focalization distance, lens tilt angle (with respect to the xy plane) (figure 1(c)), angle of rotation with respect to the x axis, electric field amplitude and pupil displacement. When the parameters are defined, they are used to calculate the minimum Gaussian beam width, Rayleigh range, the curvature radius at the initial plane and the Gouy phase.

One of the most important steps in the simulation is the definition of the matrix dimensions. The matrix dimensions are relevant at doing the propagation because small dimensions compared with the beam width makes the beam to be a dot around the beam waist. Contrary, too large dimensions makes it visible but with lack of resolution. Then, a balance is needed to get the best dimensions to observe the intensity distribution in the different positions. Moreover, when the real intensity distribution is used, the matrix dimensions have to fit with the experimentally obtained matrix dimensions.

The program consists in simulating the propagation using the complex values of the electric field at the output of the objective and propagating them. In order to simulate the complex values, the program uses the description of a Gaussian beam (1) with the already calculated parameters.

$$E(r, z) = E_0 \frac{\omega_0}{\omega(z)} e^{\frac{-r^2}{\omega(z)^2}} e^{-i(kz + k\frac{r^2}{2R(z)} - \psi(z))}, \quad (1)$$

Where  $r$  is the radial distance from the center of the beam,  $z$  the axial distance from the beam focus,  $k$  the wave number for a wavelength  $\lambda$ ,  $E_0$  the electrical field amplitude at the origin,  $\omega(z)$  is the beam width at  $z$ ,  $\omega_0$  is the beam waist radius,  $R(z)$  the radius of curvature of the beam wavefront at  $z$  and  $\psi(z)$  the Guoy phase at  $z$ .

In order to add the tilt objective effects the tilt direction values ( $x$  values in the case that tilt direction was  $x$ ) are multiplied by the cosine of the tilted angle in order to satisfy the trigonometric relation shown in figure 1(c). Furthermore, the optical path has to be taken into account, and for that reason we have to add a phase depending on the position (2).

$$E_{\text{tilt}} = E(r, z) e^{ikx \text{tg}(\alpha)} \quad (2)$$

Where  $\alpha$  is the tilted angle and the tilt is supposed to be in  $x$  direction. The tilt can be produced at different directions than our chosen axis. This is contemplated and solved by doing a change of coordinates. In the case of using the real intensity distribution, and not the Gaussian approximation, a MATLAB program (Appendix B) is used to replace the simulated values for the real ones. As the tilt is small, the tilted intensity distribution is very similar to the non-tilted one. Thus, we approximate them to be equals.

Once we have the Gaussian beam, it is cut by the circular pupil and the module of the electric field's values are recalculated to fulfill the laser pulse energy. At this point we have simulated the values of the electric field at the output of the objective. In order to know the values at some position, the propagation function is used.

The propagator cannot be a usual Fourier transform propagator because of the three orders of magnitude's difference between the output of the lens's beam width and the minimum beam width (at the focus). The propagation function which receives propaga\_d name (Appendix C) has the advantage of doing only one Fourier transform, which makes it more efficient, and the change of the scale. The propagator is based on Fresnel diffraction equations [5] and the changing of scale at calculating the propagation is crucial for the simulation.

## 2. Results and discussion

Nine microarrays, containing six rows of five spots each, were printed on the described titanium surface where the ablation is produced at six different positions around the beam waist. For each microarray the position of the substrate was varied 1  $\mu\text{m}$  from one row to another (going from around 3  $\mu\text{m}$  above the beam waist to 2  $\mu\text{m}$  below). For each microarray, the energy has also changed (going from 7.5 nJ for each pulse up to 2  $\mu\text{J}$ ). The spots produced by the laser beam on the titanium layer were observed under an optical microscope to check the properties and to measure their dimensions. The obtained images are presented in figure 3.

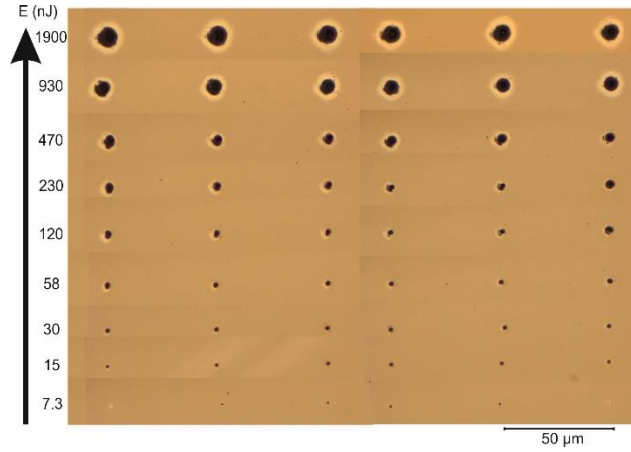


Figure 3. Optical microscopy images of one selected row of each microarray. The position with respect to the beam waist of each column changes 1  $\mu\text{m}$  from one to another, going from around 3  $\mu\text{m}$  above (leftmost) to 2  $\mu\text{m}$  below (rightmost). All the spots in each row were ablated at the laser pulse energy indicated in the left part of the image.

The spots are roughly circular and have a different shape depending on the focusing position. The spots obtained at low pulse energy are rather uniform, but those obtained at high energies present some rings or part of rings (depending on the energy). These small rings appear by diffraction because the beam is cut by the objective aperture. Titanium spots radius increases with the laser pulse energy and spots with 600 nm of radius are obtained at the lowest energies. This is smaller than the diffraction limited spot (1139 nm radius) for the laser wavelength at 1027 nm. Titanium spots can be used to determine the dimensions of the beam on the sample and the fluence ablation threshold of titanium. The microarrays used in the analysis corresponds to low pulse energy, where the local fluence of the rings is lower than the fluence threshold and, therefore, the rings are not observed in the spots.

The local fluence (energy per unit area) distribution for a Gaussian laser beam (figure 2(a)) is given by

$$F(r) = \frac{2E_{in}}{\pi\omega^2} e^{-2r^2/\omega^2}, \quad (3)$$

where  $r$  is the spot radius,  $E_{in}$  the laser pulse energy and  $\omega$  the beam radius (distance around the beam axis from which the local fluence decreases a factor  $1/e^2$ ).

Accordingly, and assuming that titanium has a laser ablation threshold  $F_0$  the radius of the spots should scale with laser pulse energy as:

$$r^2 = \frac{\omega^2}{2} \left( \ln E_{in} - \ln \frac{\pi\omega^2 F_0}{2} \right) \quad (4)$$

This relationship gives rise to the representation of the square radius of the spots vs the logarithm of the energy presented in figure 4(a). The spots dimensions were determined using appropriate software to identify the circle best suited to the spot perimeter. The figure represents a clear linear dependence. From this dependence the values of  $F_0$  and  $\omega$  can be obtained. These are, respectively,  $0.25 \text{ J/cm}^2$  and  $0.9 \text{ }\mu\text{m}$ .

The  $F_0$  and  $\omega$  were not only calculated on the beam waist, but on different six positions. The fluence threshold calculated using the different positions is the same with an error of  $0.05 \text{ J/cm}^2$ . The evolution of the different  $\omega$  in function of the position with respect to the beam waist is presented in figure 4(b) (the beam waist position ( $z=0$ ) was chosen taking into account the evolution of the beam width).

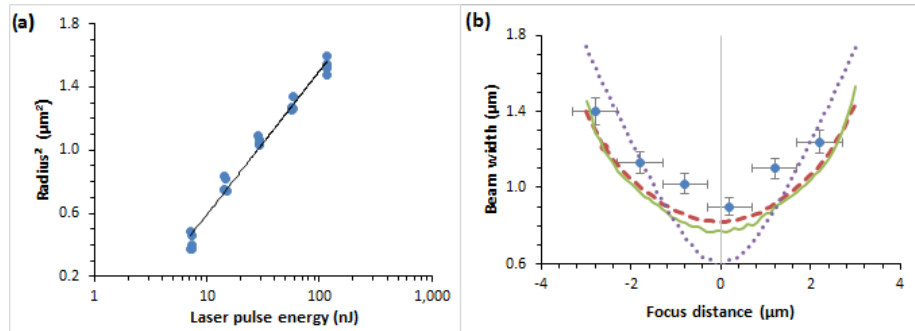


Figure 4. (a) Plot of the radius squared of the laser spots vs laser pulse energy. (b) Plot of the beam width along the z-axis where (●) are the experimental values, (···) the ideal propagation without neither tilt nor pupil, (---) the simulation values using the Gaussian beam approximation,  $0.7^\circ$  tilt angle and  $0.4 \text{ mm}$  of pupil displacement. The continuous line correspond to the simulation using the real intensity distribution and the same tilt and pupil values.

At studying the evolution of the beam intensity distribution the results obtained are not enough to characterize the beam profile propagation because they are too close to the beam waist. At these positions the energy is highly concentrated and it implies ablation at all the energies without distinguishing the intensity distribution details. Therefore, six different microarrays, involving 21 rows of five spots each, were printed on the described titanium surface where the ablation is produced at twenty-one different positions around the beam waist. For each microarray the position of the substrate was varied  $4 \text{ }\mu\text{m}$  from one row to another (going from around  $40 \text{ }\mu\text{m}$  above the waist to  $40 \text{ }\mu\text{m}$  below). For each microarray, the energy was also changed (going from  $0.3 \text{ }\mu\text{J}$  for each pulse up to  $4.8 \text{ }\mu\text{J}$ ). The spots produced by the laser beam on the titanium layer were observed under an optical microscope to check the properties and to measure their dimensions. The obtained images are presented in figure 5.

In all the microarrays, the dimensions of the spots increase with the laser pulse energy. For a fixed laser pulse energy, the spots dimensions increase as higher is the distance from the beam waist. But this increase of dimension reaches a maximum at certain position  $\Delta x_{\text{max}}$ , and after this position the ablated area decreases.  $\Delta x_{\text{max}}$  is smaller the lower the energy of the beam is and follows equation (4). Therefore, at energies lower than  $30 \text{ nJ}$  (figure 3), the highest area point is produced at the beam waist position and this area decreases with the distance.

Spots are obtained with good reproducibility, and the intensity distribution is well defined. Thus, it is possible to study the differences between the normal Gaussian beam and our modified Gaussian beam. The spots morphology are different if the substrate is below the beam waist or above it. On the above beam waist positions, the spots are roughly circular, with strange morphologies in the center and with several rings. These rings are not completely circular, in fact, they seem to be flattened in its right side, and their intensity distribution is centered. On the positions below, the spots are elliptical and present clear elliptical rings. At these positions, the

pick intensity and intensity distribution are clearly displaced to the top-right, but there is remaining intensity at the center which is visualized as a dot or ring (depending on the energy and position).

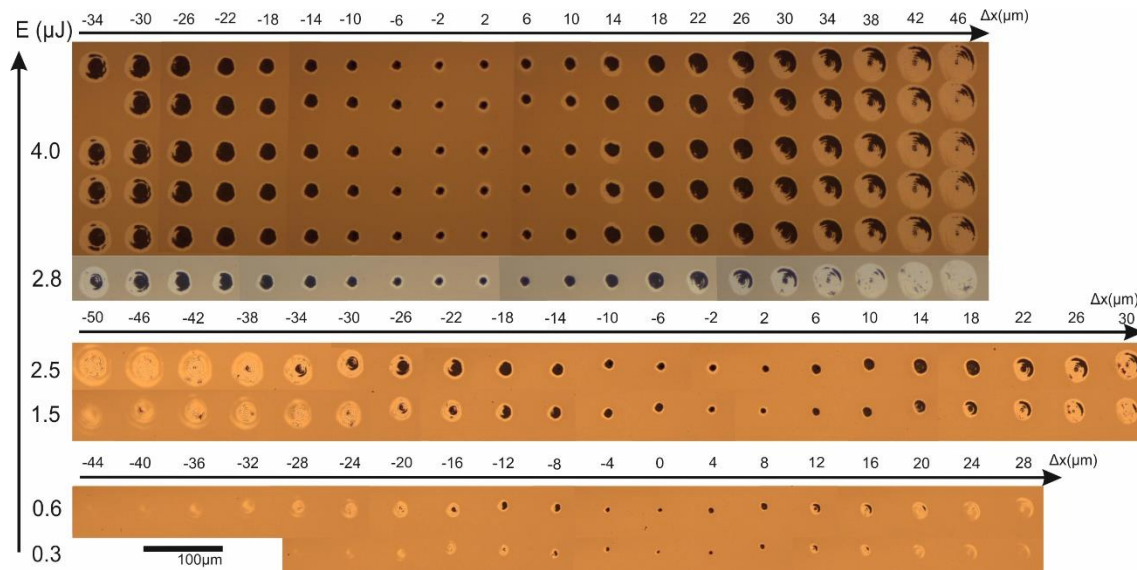


Figure 5. Optical microscopy images of one selected row of each microarray and the complete microarray produced at the highest laser pulse energy. The position with respect to the beam waist of each column is indicated at the top part, where (-) means below the beam waist and (+) above it. All the spots in each row were ablated at the laser pulse energy indicated in the left part of the image.

With the aim of explaining these differences in morphology, the program in MATLAB (Appendix A) is used to simulate the propagation. In this program we have four free parameters: aperture  $xy$  position, objective tilt angle with respect to the beam propagation direction and the  $xy$  axis rotation. We can also determine the impact of having or not the pupil.

First of all, the behaviors of the beam when using or not aperture and the intensity profile response at displacing it are studied (figure 6). The presence of the aperture generates a ring diffraction pattern in the beam intensity distribution. At some positions, instead of having the intensity pick at the middle, as it is produced in a normal Gaussian beam, it is in a circular ring around the middle. Therefore, we determine that the aperture is the responsible of the rings we observe in the experiments. However, the experimentally observed rings have not the same intensity at all of the regions. In fact, the intensity is deviated to one side. When we simulate a displacement of the aperture with the beam, we observe a similar behavior (figure 6). The deviation of the intensity profile is directly proportional to the aperture displacement. As the beam is circular and the aperture is circular too, the deviation direction has no relevance because of the symmetry. At displacing 0.2 mm the intensity displacement effect is unappreciable. At 0.4 mm the effect is well defined and this effect is more notable as we increase the distance, but with distances higher than 0.6 mm the circularity is lost. This aperture simulations helped to understand why and how are produced the rings. However, taking into account only the aperture, the morphology would be the same before and after the focalization point and this does not happen.

When the experiment was done, it was appreciated that the objective slightly deviates the beam. In other words, it slightly changes the beam propagation direction. This suggests a possible lens tilt. Thus, that tilt is simulated (figure 7). The effect of a tilted lens is to make the beam more and more elliptical, in the direction of the tilt, as we are nearer to the beam waist. The same behavior, but totally perpendicular, is produced after being focalized. This elliptical phenomena is only produced in the 60  $\mu\text{m}$  around the focalization point, and out of this range the simulated intensity distribution is completely circular. Comparing the simulation and the experimental spots, we

determine that the objective rotation is around 26 degrees with respect to the x axis. The simulation does not fits the elliptical intensity distribution measured using a ccd camera (figure 2(b)). However, this elliptical distribution may be produced due to the tilt and may be explained using less approximations.

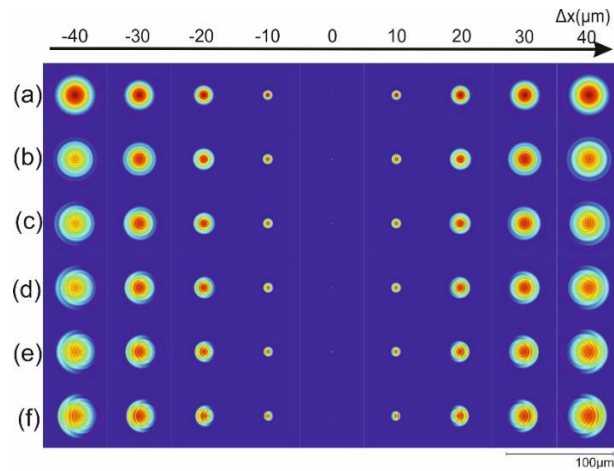


Figure 6. Plot of the simulated laser beam intensity distribution around the beam waist (a) without pupil, (b) with a centered pupil, (c) with 0.2 mm, (d) with 0.4 mm, (e) with 0.6 mm and (f) with 0.8 mm right-displaced pupil. The position with respect to the beam waist of each column is indicated at the top part, where (-) means below the beam waist and (+) above it.

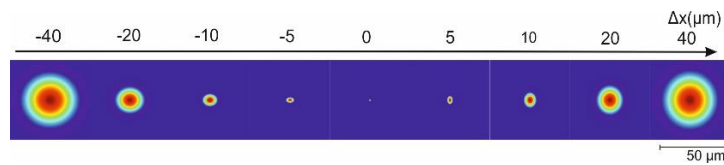


Figure 7. Plot of the simulated laser beam intensity distribution around the beam waist using  $0.7^\circ$  tilted objective in x direction. The position with respect to the beam waist of each column is indicated at the top part, where (-) means below the beam waist and (+) above it.

Once we observe the different distributions above and below the waist, we add the presence of a centered pupil. The propagation is simulated for different angles (figure 8) obtaining a variety of morphologies. From  $0^\circ$  up to  $0.3^\circ$ , there is a comfort zone where no changes in the intensity profile are produced. From  $0.3^\circ$  to  $0.6^\circ$  the intensity is higher in the tilt axis with respect to the perpendicular, but there are still appearing circular rings in the middle. From  $0.6^\circ$  to  $0.8^\circ$  the middle circular ring has been converted into a  $45^\circ$  tilted square with intensity picks at the vertexes. Higher than  $0.8^\circ$  the morphologies start to be more difficult to explain and more irregular.

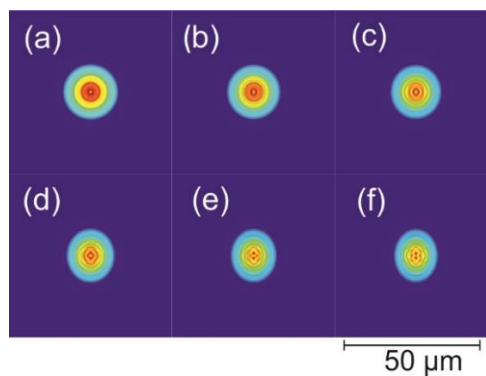


Figure 8. Plot of the simulated laser beam intensity distribution around the beam waist using a centered pupil and (a)  $0^\circ$ , (b)  $0.3^\circ$ , (c)  $0.5^\circ$ , (d)  $0.7^\circ$ , (e)  $0.8^\circ$  and (f)  $0.9^\circ$  tilted objective in x direction at .

The objective tilt was measured taking into account the beam deviation and the distance between the measurement position and the objective entrance. This tilt has a value of  $0.7 \pm 0.05^\circ$ . The propagation through this  $0.7^\circ$  tilted lens and 0.4 mm pupil deviation in the same rotation direction was simulated and compared with the experiment (figure 9). The simulation was done using a circular perfectly collimated Gaussian beam, and also using the intensity profile obtained in the experiment (figure 2 (a)). Both simulations are very similar, which corroborate the Gaussian beam approximation. The morphology of the intensity distribution is similar to the experimental one at all of the regions, before and after the beam waist. Before the beam waist, we see some distribution that coincides (figure 10(a)) and the center shape can only be explained in this simulation taking into account the  $0.7^\circ$  lens tilt. After the focalization of the beam, the beam presents a perfect defined rings, but the smallest ring is not as perfect and it is similar to the simulation (figure 10(b)). Comparing the simulation and the experiment we deduce that the objective is tilted and displaced in the same direction. The pupil displacement might be produced to compensate the tilt. Therefore, when the tilt will be solved, the displacement will also be solved.

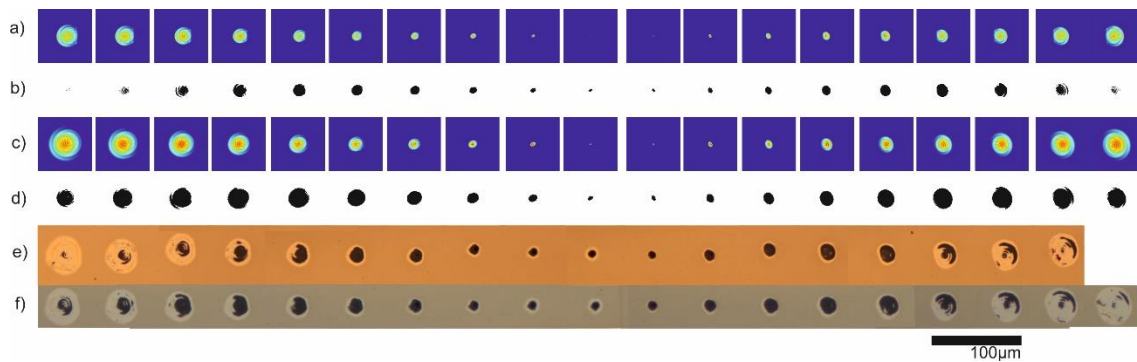


Figure 9. Plot of the simulated laser beam intensity distribution around the beam waist using (a) the real intensity distribution and (c) the Gaussian beam approximation. Plot of the simulated energy threshold using 2.5  $\mu\text{J}$  laser pulse energy using the (b) real intensity distribution and (d) the Gaussian beam approximation. Optical microscopy images of a selected row of the microarrays with (e) 2.5  $\mu\text{J}$  and (f) 2.8  $\mu\text{J}$  laser pulse energy. The position with respect to the beam waist of each column changes 4  $\mu\text{m}$  from one to another, going from around 38  $\mu\text{m}$  above (leftmost) to 34  $\mu\text{m}$  below (rightmost).

Using this simulation parameters, the  $\omega$  was calculated at positions near to the focalization point, with the two possible intensity distributions (Gaussian and experimental distributions). The  $\omega$  was also simulated at the same positions in the case that there had neither tilt nor pupil. The different  $\omega$  in the different cases are represented in figure 5(b). The experimentally obtained  $\omega$  follow the same evolution and have a similar value than the simulated cases. Minimum  $\omega$  varies from 0.6  $\mu\text{m}$  to 0.9  $\mu\text{m}$  from the ideal to the real propagation. Rayleigh distance has also changed from 1.1  $\mu\text{m}$  to  $2.3 \pm 0.2 \mu\text{m}$ .

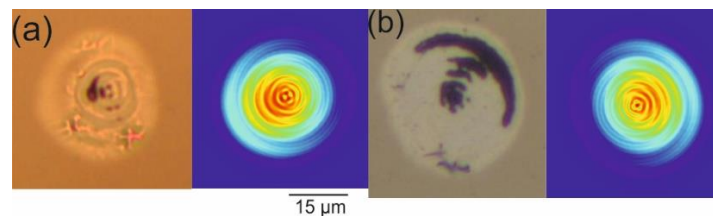


Figure 10. Plot of the simulated laser beam intensity and optical microscopy image of a selected spots with (a) 2.5  $\mu\text{J}$  laser pulse energy at 30  $\mu\text{m}$  above and (b) 30  $\mu\text{m}$  below the beam waist with 2.8  $\mu\text{J}$  pulse.

In order to simulate the titanium-light interaction and the ablation, the already calculated fluence threshold is supposed. This  $F_0$  takes the value of  $0.25 \text{ J/cm}^2$  and it is supposed that higher fluences would ablate the titanium and lower fluences would not. The ablated titanium simulation is represented in Fig.9. The threshold simulation using the real beam distribution is very similar to

the experimentally obtained spots. We observe that the energy and the energy distribution coincides with the experiments because the simulated spots have similar morphology and dimensions than the experimental ones. When the Gaussian beam approximation is used, the spots are bigger than the experimental ones. This is produced because the energy is more concentrated in the Gaussian beam case than the real one. However, if we use a higher threshold, the simulated spots (using the Gaussian beam approximation) are equal than the experimental ones. Although the simulation and the experiment coincides, in the experimentally obtained spots a pick intensity appears on the right which is not seen in the simulation. The peak intensity, which seem a bow, is at the same position (right of the spot) before the beam waist and after it. The fact of being at the same side before and after the focalization point cannot be explained using this simulation.

### 3. Conclusion

The observation by means of optical microscopy of the microarrays reveals well defined spots with good reproducibility. Therefore, the laser intensity distribution is almost the same for all the pulses and it will be the same in following experiments. The analysis of the dimensions of the spots reveals the fact that smaller than the diffraction limited spot for the laser wavelength at 1027 nm can be obtained using this laser. Moreover, the Rayleigh range and the beam waist dimensions are higher (2.3 $\mu$ m and 0.9 $\mu$ m) than the ideal case where neither pupil nor tilt are contemplated.

Comparison of the simulations with the experiment shows that the apparition of rings and the displacement of the intensity profile is caused by the presence of a pupil and a displacement of the objective with respect to the beam. Furthermore, the tilted objective makes the beam elliptical. However, for tilt angles smaller than 0.3° the beam has no appreciable changes in the distribution. The experimental-simulation similarity reveals that the objective is tilted 0.7° and displaced around 0.4 mm in the same direction (26° with respect to the x axis).

Slight differences are observed between the simulations and the experimental results. In order to improve the matching between them, the objective should be further characterized by taking it out of the setup and studying the behavior of the light going through it at changing parameters, tilt angle and objective displacement.

### Acknowledgments

The advisor work of Dr J. M. Fernandez-Pradas is greatly acknowledged, as well the assistance of Dr S. Bosch in the simulations. Many thanks also to F. Caballero-Lucas and the other laboratory colleagues for the assistance in the laboratory.

### References

- [1] C. B. Arnold and A. Pique, 2007. Laser Direct-Write Processing *MRS Bulletin* **32**, 915.
- [2] F. Caballero-Lucas, C. Florian, J.M. Fernández-Pradas, J.L. Morenza and P. Serra, 2016. Beam waist position study for surface modification of polymethyl-methacrylate with femtosecond laser pulses *Appl. Surf. Sci.* **374**, 353-358.
- [3] M. Colina, M. Duocastella, J. M. Fernández-Pradas, P. Serra, and J. L. Morenza, 2006. Laser-induced forward transfer of liquids: Study of the droplet ejection process *J. Appl. Phys.* **99**, 084909.
- [4] C. Florian, F. Caballero-Lucas, J. M. Fernández-Pradas, S. Bosch, J. L. Morenza and P. Serra, 2015. Femtosecond laser surface ablation of polymethyl-methacrylate with position control through z-scan *J. Phys. D: Appl. Phys.* **48**, 335302
- [5] J. W. Goodman, 1996 *Introduction to Fourier Optics* (New York: McGraw-Hill), Chapter 4.